Interrogation of orbital structure by elliptically polarized intense femtosecond laser pulses

M. Abu-samha[1] and L. B. Madsen[2]
[1]*Department of Chemistry, University of Bergen, Postboks 7803, N-5020 Bergen, Norway*
[2]*Lundbeck Foundation Theoretical Center for Quantum System Research, Department of Physics and Astronomy, Aarhus University, DK-8000 Aarhus C, Denmark.*
(Received 31 May 2011; published 22 August 2011)

We solve the three-dimensional time-dependent Schrödinger equation and present investigations of the imprint of the orbital angular node in photoelectron momentum distributions of an aligned atomic p-type orbital following ionization by an intense elliptically polarized laser pulse of femtosecond duration. We investigate the role of light ellipticity and the alignment angle of the major polarization axis of the external field relative to the probed orbital by studying radial and angular momentum distributions, the latter at a fixed narrow interval of final momenta close to the peak of the photoelectron momentum distribution. In general only the angular distributions carry a clear signature of the orbital symmetry. Our study shows that circular polarization gives the most clear imprints of orbital nodes. These findings are insensitive to pulse duration.

DOI: 10.1103/PhysRevA.84.023411 PACS number(s): 32.80.Rm

I. INTRODUCTION

Experiments are now emerging on strong-field ionization of atomic and molecular targets by circularly and elliptically polarized femtosecond laser pulses [1–5]. For an elliptically polarized laser, the field has two perpendicular components, and the electron dynamics and the resultant momentum distributions depend on the relative magnitudes of the field components (light ellipticity), pulse duration (few-cycle vs many-cycle ionization regimes), and carrier-envelope phase (CEP); see, for example, the reviews [6,7] and references therein.

Strong-field experiments based on elliptically polarized light reveal new and exciting phenomena [1–8]. Recently, measurements of the momentum distributions from the He atom probed by a few-cycle elliptically polarized laser [2] revealed an angular shift in the momentum distributions relative to the classical predictions obtained by the simple-man's model, in which the final momentum of a continuum electron born at time t_i is given by (in atomic units, which are used throughout)

$$\vec{k}_f = -\int_{t_i}^{\infty} \vec{E}(t')dt' = -\vec{A}(t_i), \tag{1}$$

where $\vec{A}(t)$ is the vector potential and $\vec{E}(t) = -\partial_t \vec{A}(t)$ the electric field. For a few-cycle pulse of duration T and with a CEP value of zero, electron emission at the peak of the pulse ($t = T/2$) dominates the ionization process, and the dominant final momentum within this model is thus $\vec{k}_f = -\vec{A}(T/2)$. In a recent numerical study of the momentum distributions from the H($1s$) state in circularly polarized laser pulses [9], the numerical results support the experimental observations of [2], and the discrepancy between measurements and classical predictions of the final electron momentum was attributed to the interplay between the Coulomb potential and the external field. In the many-cycles regimes such shifts were observed quite some time ago [10] and at the time were explained in terms of the Coulomb field [11–13]. Also, more recent works invoke the Coulomb shift [14].

In more recent experiments [1,4,15,16], photoelectron momentum distributions, obtained by probing three-dimensional (3D)-oriented [17–20] polar molecules by intense many-cycle circularly polarized laser pulses, were shown to reflect permanent dipole moments and polarizabilities of the probed orbitals, in addition to their angular nodes. The use of circularly polarized light in these studies entails a cleaner ionization signal than is the case with the use of linearly polarized light. This advantage occurs because in circularly polarized fields the electron is monotonically driven away from the target while in the case of linearly polarized light the electron may be driven back to rescatter with the core as the laser field changes its direction; circular polarization switches off rescattering [21]. In Refs. [1,4,15,16], it is demonstrated how nodes of molecular orbitals directly map to nodes in the photoelectron momentum distributions when using circularly polarized light. The observation of angular nodes in photoelectron momentum distributions has also been predicted by theoretical calculations [22], based on both the strong-field approximation [23,24] and numerical solution of the 3D time-dependent Schrödinger equation (TDSE) for circularly polarized laser pulses. The physics behind this phenomenon is illustrated in Fig. 1, where we use the Ar($3p_x$) state as an example. In Fig. 1(a) the electron density and the driving field (at the peak of the pulse) are shown in the polarization plane of a many-cycle circularly polarized laser pulse. From the theory of tunneling in a circularly polarized field [25], the emission rate depends on the angular density profile of the probed orbital: Whereas the emission rate is largest when the electric field points in the direction where the electron density is maximum [along $\hat{x}$ in Fig. 1(a)], it is greatly reduced in the direction of the angular node [along $\hat{y}$ in Fig. 1(a)] due to vanishing electron density. From the simple-man's model, see Eq. (1), the electrons emitted when the electric field points along $\hat{x}$ ($\hat{y}$) are detected in the momentum distributions along k_y (k_x) simply because the electric field and the vector potential are $\pi/2$ out of phase. Accordingly, the reduced electron emission from the angular node of the Ar($3p_x$) state (when the electric field of the circularly polarized field points along $\hat{y}$) is manifested in the momentum distributions as a suppressed

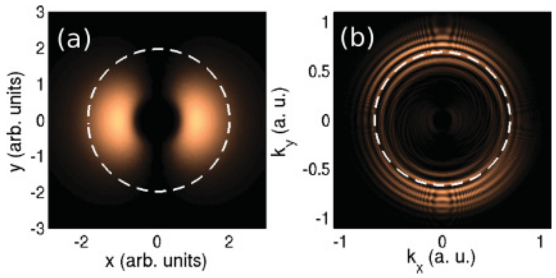

FIG. 1. (Color online) (a) Electron density for the Ar($3p_x$) state together with the peak electric field (dashed curve) of a circularly polarized laser pulse containing seven optical cycles with peak intensity of 1.06×10^{14} W/cm^2. (b) Momentum distribution following the interaction of the Ar($3p_x$) state with the external field, illustrated in (a). In (b), the vector potential at the peak of the pulse is illustrated by the dashed curve.

differential ionization probability along k_x. These predictions are indeed corroborated by numerical TDSE calculations of the momentum distribution for the Ar($3p_x$) state, shown in Fig. 1(b) (see Sec. II for computational details).

In the present work, we explore the application of femtosecond laser pulses of general elliptical polarization in the interrogation of orbital symmetry (angular nodes) in strong-field ionization of an aligned p-type orbital. So far only the limiting cases of linear and circular polarized light pulses have been considered in this context. We investigate in particular how the photoelectron momentum distribution depends on light ellipticity and alignment of the major polarization axis of the external field relative to the probed orbital. The effect of pulse duration (few-cycle vs many-cycle pulses) is also addressed. Our approach is based on numerical solution of the 3D TDSE. This approach is computationally expensive, and to simplify the calculations as much as possible while still representing the essential aspects of the problem, we follow [22] and use aligned atomic orbitals in argon to mimic an aligned molecular orbital. With this abstraction, we can treat the problem in a well-established single-electron approximation using a well-tested argon model potential [26]. Specifically, we represent the probed orbital by the Ar($3p_x$)/Ar($3p_y$) state, and provide comparisons with TDSE results for the rotationally invariant H($1s$) state at the same laser parameters to address the question to which extent the momentum distributions reveal the nodes of the p orbitals, and if these investigations favor a particular light ellipticity.

We are mainly interested in the ellipticity range at which electron rescattering is minimal. Photoelectron momentum distributions are computed at four light ellipticity values in the range between $\pi/2$ (circular polarization) and $\pi/4$. For the Ar($3p_x$) [Ar($3p_y$)] state, the calculations are performed at parallel [perpendicular] alignment of the major polarization axis of the external field relative to the probed orbital, and the distribution is strongly dependent on this alignment angle. We consider the radial momentum distribution and the angular momentum distribution for momentum magnitude in a narrow band around the peak in the distribution. We found that this latter quantity is more sensitive to the orbital symmetry than the radial distribution for a larger range of ellipticities away from the circular one. The optimal choice for light ellipticity is circular, in which case signatures of the orbital nodes appear most clearly in the angular distribution.

The paper is organized as follows. The laser parameters and the computational details are given in Sec. II. The results and discussion are presented in Sec. III, and the summary is provided in Sec. IV.

II. LASER PARAMETERS AND COMPUTATIONAL DETAILS

The elliptically polarized laser field is defined as $\vec{E}(t) = -\partial_t \vec{A}(t)$, where $\vec{A}(t)$ is the vector potential

$$\vec{A}(t) = A_0 f(t) \begin{pmatrix} \cos(\omega t + \phi)\cos(\epsilon/2) \\ \sin(\omega t + \phi)\sin(\epsilon/2) \\ 0 \end{pmatrix}, \tag{2}$$

with A_0 the amplitude, ω the carrier frequency, ϕ the CEP, ϵ the light ellipticity [$\epsilon = \pi/2$ (0) for circular polarization (linear polarization along $\hat{x}$)], and $f(t) = \sin^2(\omega t/2N)$ is a sine-squared envelope for the N-cycle pulse. In the present study, the laser intensity is fixed at 1.06×10^{14} W/cm^2, the angular frequency $\omega = 0.057$ a.u. corresponding to 800 nm light, and $\phi = -\pi/2$. The calculations are performed using laser pulses with both $N = 3$ and $N = 7$ optical cycles, and at ϵ values of $\pi/2$, $11\pi/25$, $\pi/3$, and $\pi/4$. For $N = 3$ there are strong CEP effects. For $N = 7$ the pulse is already long enough that CEP effects are minor (see below).

The wave function is expressed in spherical harmonics as

$$\Psi(\boldsymbol{r},t) = \sum_{l=0}^{l_{\max}} \sum_{m=-l}^{l} \frac{f_{lm}(r,t)}{r} Y_{lm}(\Omega), \tag{3}$$

and the TDSE is solved in the velocity gauge with a grid representation for the reduced radial wave functions $f_{lm}(r,t)$ [27]. The expansion in Eq. (3) is truncated at $l_{\max} = 40$ [angular basis set containing $(l_{\max}+1)^2 = 1681$ functions] and the results are checked for convergence. The single-active-electron (SAE) potential describing Ar is taken from Ref. [26]. We use an equidistant grid with 4096 points that extends up to 400 a.u. A propagation time step of 0.005 a.u. is used. The momentum distributions are computed by projection on scattering states of the field-free potential [28]. Here, we present momentum distributions in the polarization plane of the external field, that is, $dP/d\vec{k}$ with the polar angle θ_k fixed at $\pi/2$ corresponding to the (k_x,k_y) plane.

III. RESULTS AND DISCUSSION

An important aspect of this work is to investigate the possibility of obtaining direct information about the orbital structure of oriented targets by strong-field ionization with elliptically polarized laser pulses. Toward this end, we investigate the momentum distributions of an aligned atomic p-type orbital, represented here by the Ar($3p_x$)/Ar($3p_y$) orbital, and compare to the rotationally invariant H($1s$) state.

A. Rotationally invariant H(1s) state as initial state

We begin by discussing the momentum distributions computed for the H($1s$) initial state at a range of ellipticity

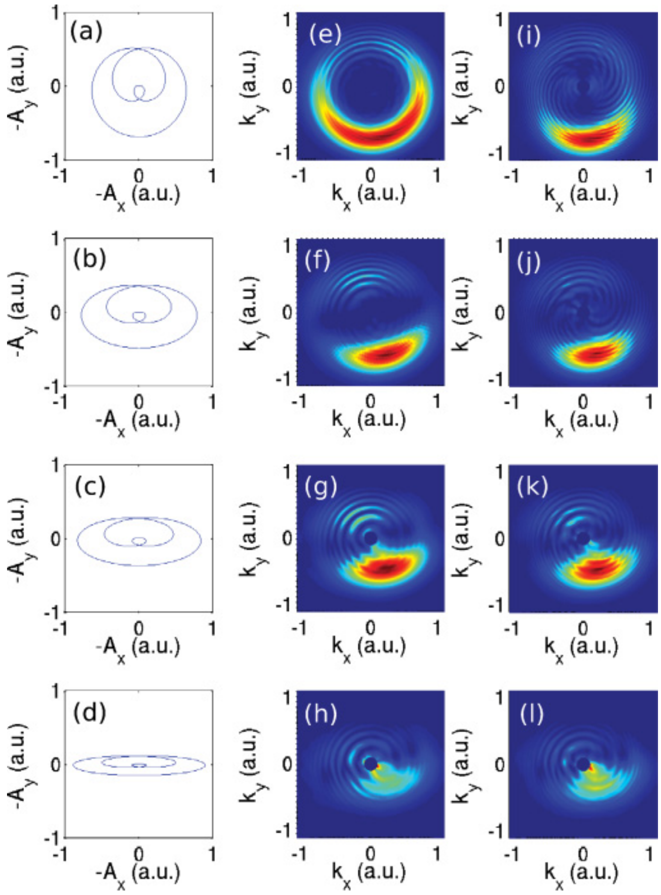

FIG. 2. (Color online) Parametric plots of the prediction of the final momentum according to Eq. (1), i.e., the negative of the vector potentials (left column). The momentum distributions as obtained from the TDSE calculations are shown for H initially in the $1s$ state (middle column) and for Ar initially in the $3p_x$ state [right column, see illustration in Fig. 3(a)] in the polarization plane of an elliptically polarized field with light ellipticity $\epsilon = \pi/2$ (top row), $11\pi/25$ (second row), $\pi/3$ (third row) and $\pi/4$ (bottom row). The momentum scale is linear in all plots. The laser pulses contain three optical cycles, $\omega = 0.057$ a.u. (800 nm), the CEP value is $\phi = -\pi/2$, and the peak intensity is 1.06×10^{14} W/cm^2.

values and for 800-nm laser pulses containing three optical cycles. Since the H($1s$) state is rotationally invariant, rotating the major polarization axis of the external field only results in an overall angular shift of the momentum distribution (see Refs. [29,30] for a discussion of the case of circular polarization). The external field is defined in Eq. (2) such that the major polarization axis coincides with $\hat{x}$.

In Fig. 2 we show parametric plots of the vector potentials [(a)–(d)] and the corresponding 2D momentum distributions [(e)–(h)]. For the H($1s$) initial state at $\epsilon = \pi/2$ [Fig. 2(e)] the momentum distribution is characterized by a main emission peak, characteristic of tunneling ionization at the peak of a short pulse [31–33]. Notice that at $k_y > 0$ the momentum distribution shows rings due to multiphoton absorption at lower-intensity half cycles. [For a three-cycle pulse, the spectral bandwidth is $\Delta\omega \approx \omega/3$, and for the H($1s$) state at the present laser intensity and $\epsilon = \pi/2$ the Keldysh parameter [34] is $\gamma = 1.46$.] The main emission peak (at $k_y < 0$) is rotated relative to the classical predictions of the final momentum based on the simple-man's model (1) in which $\vec{k}_f = -\vec{A}(T/2) = -A_y$, cf. Fig. 2(a). The discrepancy between the numerical results and the classical predictions is mainly due to the interplay between the atomic potential and the external field [9]. From the momentum distribution, one can see that the probability of finding electrons with low momenta (0.1 $< \vec{k}_f <$ 0.5 a.u.) is essentially zero, indicating that at $\epsilon = \pi/2$ the continuum electron is progressively driven away from the core by the external field and that the electron rescattering channel is indeed closed, in accordance with the prediction of classical physics.

For the H($1s$) initial state at $\epsilon = 11\pi/25$ and $\pi/3$ in Figs. 2(f) and 2(g), respectively, multiphoton absorptions rings are present in the momentum distributions at $k_y > 0$ [at the present laser intensity, the Keldysh parameter (γ) values at $\epsilon = 11\pi/25$ and $\pi/3$ are 1.35 and 1.2, respectively). The momentum distributions show a main emission peak at $k_y < 0$ due to tunneling ionization at the peak of the pulse. However, the final electron momentum of the main emission peak is progressively smaller, compared to the calculations at $\epsilon = \pi/2$. This latter feature is understood based on the classical predictions of the final momentum: From the negative vector potentials shown in Fig. 2 (left column) and according to the simple-man's model (1), the magnitude of the final momentum (k_f) is 0.68, 0.62, and 0.48 a.u. for $\epsilon = \pi/2$, $11\pi/25$, and $\pi/3$, respectively. These values for the final momenta are comparable to those obtained from TDSE calculations: Electron momenta with maximum differential probability are 0.80, 0.72, and 0.57 a.u. at $\epsilon = \pi/2$, $11\pi/25$, and $\pi/3$, respectively. Notice that the classical predictions underestimate the final momentum at the present laser parameters, and that the discrepancy between the TDSE calculations and the classical predictions of k_f is rather insensitive to the light ellipticity. Moreover, we note that the angular shift of the momentum distribution compared to the $k_x = 0$ line expected from the simple-man's model increases by going to smaller ϵ values: The angular shifts for H are 9° at $\epsilon = \pi/2$; 17° at $11\pi/25$; and 26° at $\epsilon = \pi/3$, from the present numerical calculations. From Fig. 2, one can also see that the probability of finding low-momentum electrons is still small compared to the main emission probability for ϵ in the range $[\pi/2;\pi/3]$.

Turning to the H($1s$) initial state at $\epsilon = \pi/4$ in Fig. 2(h), the emission pattern observed at light ellipticity in the range $\epsilon \in [\pi/2;\pi/3]$ is now distorted by rescattered electrons and carries a clear signature of low-energy electrons typical for tunneling ionization by the linear component of the external field [31]. [The Keldysh parameter $\gamma = 1.04$ for the H($1s$) state in a linearly polarized laser pulse of the present intensity.] Because of these rescattering induced features, it is no longer meaningful to discuss the angular shift at $\epsilon = \pi/4$. The final electron momentum is 0.47 a.u. from numerical calculations, compared to 0.37 a.u. from classical predictions based on the simple-man's model of Eq. (1).

B. Ar($3p_x$) initial state: Parallel alignment of the major polarization axis and the probed orbital

We now turn to the momentum distributions for the Ar($3p_x$) state. Unlike for the H($1s$) state, the electron dynamics and

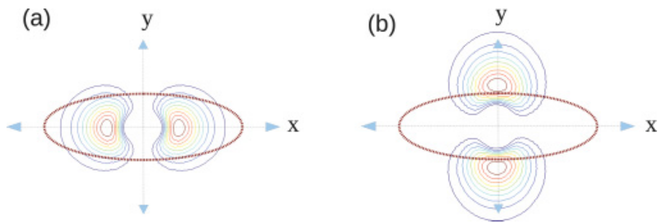

FIG. 3. (Color online) (a) Parallel and (b) perpendicular alignment of the major polarization axis of an elliptically polarized laser pulse (red dotted curves) relative to the (a) Ar($3p_x$) and (b) Ar($3p_y$) initial orbitals whose densities are displayed by the thin contour lines. To facilitate comparison to the results for the H($1s$) initial state, we fix the laser polarization axis along $\hat{x}$ and rotate the orbital going from the case of (a) parallel to (b) perpendicular alignment.

momentum distributions for the Ar($3p_x$) state are sensitive to the alignment of the major polarization axis of the external field relative to the orbital. We first consider the parallel alignment of the major polarization axis of an elliptically polarized laser pulse relative to the Ar($3p_x$) orbital, corresponding to the scenario demonstrated in Fig. 3(a). The resulting 2D momentum distributions are shown in Fig. 2 (right column) for ellipticity values in the range $\epsilon \in [\pi/2;\pi/4]$. Notice that since the peak electric field coincides with $\hat{x}$, lowering the light ellipticity would result in increasing the field strength along $\hat{x}$. For the Ar($3p_x$) state, the ellipticity-wise momentum distributions are, in general, similar to those for the H($1s$) state. The angular shifts of the peak of the momentum distributions with respect to the $k_x = 0$ line from the TDSE calculations on the Ar($3p_x$) [H($1s$)] state are 9° [9°] at $\epsilon = \pi/2$; 15° [17°] at $11\pi/25$; and 25° [26°] at $\epsilon = \pi/3$. This suggests that at the present laser parameters, the angular shift is independent of the probed system. Moreover, for the Ar $3p_x$ [H($1s$)] state, the magnitude of the final electron momentum k_f from the present TDSE calculations is 0.8 a.u. [0.8 a.u.] at $\epsilon = \pi/2$; 0.68 a.u. [0.72 a.u.] at $\epsilon = 11\pi/25$; 0.57 a.u. [0.57 a.u.] at $\epsilon = \pi/3$; and 0.45 a.u. [0.47 a.u.] at $\epsilon = \pi/4$.

A more careful look at the momentum distributions for H and Ar in Fig. 2 reveals that the distribution for Ar is more narrow angular wise than the distribution in H for circular polarization [Figs. 2(e) and 2(i)]. This difference reflects the difference in the density profiles of the H($1s$) and Ar($3p_x$) initial orbitals. While the $1s$ orbital density is isotropic with respect to variation in the azimuthal angle, the $3p_x$ orbitals density peaks in the $\pm x$ directions. The comparison of Figs. 2(e) and 2(i) shows that even though the electromagnetic field is strong enough to result in final momenta in a ring in the entire lower-half plane [Fig. 2(e)], the decrease in the electron density of the $2p_x$ orbital away from the x axis results in a more peaked distribution [Fig. 2(i)].

To study the imprint of orbital symmetry (angular nodes) in the momentum distributions of the Ar($3p_x$) state and the effect of light ellipticity in more detail, we consider one-dimensional plots of the radial [$dP/dk = \int_0^{2\pi}(dP/d\vec{k}|_{\theta_k=\pi/2})d\phi_k$] and angular [$dP/d\phi_k\ |_{k=k_0}$] electron momentum distributions. The angular distributions are computed as $\int_{k_0-\delta}^{k_0+\delta}(dP/d\vec{k}|_{\theta_k=\pi/2})k\,dk$, where k_0 is the electron momentum of maximum differential probability and $\delta = 0.05$ a.u defines the thickness of the shell around the maximum

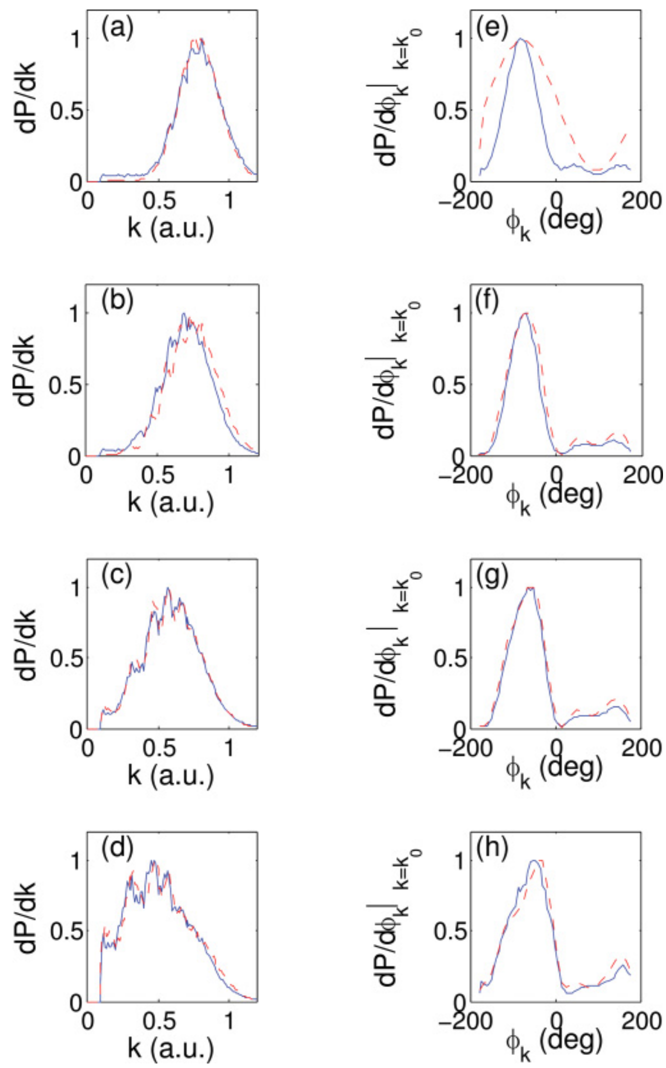

FIG. 4. (Color online) Radial momentum distributions (dP/dk, left column) and angular momentum distributions ($dP/d\phi_k\ |_{k=k_0}$, right column) for the H($1s$) state (dashed curves) and the Ar($3p_x$) state (solid curves) at ϵ values of $\pi/2$ (top row), $11\pi/25$ (second row), $\pi/3$ (third row), and $\pi/4$ (bottom row). See caption of Fig. 2 for the values of the laser pulse parameters.

value. The radial and angular distributions are shown for both the H($1s$) and Ar($3p_x$) states in Fig. 4. One can clearly see that the radial momentum distributions (left column) and their dependence on light ellipticity are very similar for the H($1s$) state and the Ar($3p_x$) state. For both systems, the radial momentum distributions show evidence of multiphoton absorption. Moreover, the radial distributions are getting broader with lowering light ellipticity: the full width at half maximum (FWHM) of the radial momentum distributions for the Ar($3p_x$) [H($1s$)] are 0.35 a.u. [0.36 a.u.] at $\epsilon = \pi/2$; 0.39 a.u. [0.4 a.u.] at $11\pi/25$; 0.42 a.u. [0.42 a.u.] at $\pi/3$; and 0.58 a.u. [0.64 a.u.] at $\pi/4$. Notice that while the FWHM increases only slightly in the range $\epsilon \in [\pi/2;\pi/3]$ it gets significantly broader at $\epsilon = \pi/4$, which could be attributed to rescattering effects which distort the momentum distributions of both states, as evident from Figs. 2(h) and 2(l). The reason why the radial distributions are so similar is because they are mainly sensitive to the long-range part of the potential, which is $-1/r$ in both H and Ar as discussed for linear polarization elsewhere [35]. This insensitivity to the short-range part of the atomic potential is enforced by the use of elliptically polarized light in the present study.

Since the radial distributions are very similar for both systems, we turn to the angular distributions in Fig. 4 (right column) for information about the orbital symmetry. At $\epsilon = \pi/2$, the angular distributions reveal the largest difference between the momentum distributions of the H($1s$) state and the Ar($3p_x$) state, in the sense that the FWHM of the angular distribution for the H($1s$) state is twice as large as that for the Ar($3p_x$) state. This difference should be large enough to allow for a clear experimental signature, and its origin is the same as discussed in detail in connection with Figs. 2(e) and 2(i) above. Going to smaller ellipticity values (other than the top row in Fig. 4) the angular distributions of the H($1s$) and Ar($3p_x$) states become very similar. The reason for this similarity is that the variation in the $3p_x$ orbital density over the angular range close to the x axis where the electric field peaks, and ionization mainly occurs, is relatively small and therefore the result is an s-like signal. Hence, in the case when the major polarization axis of the external field is aligned parallel to the probed orbital, the scenario illustrated in Fig. 3(a), information about the orbital symmetry (angular nodes) can only be obtained from the photoelectron momentum distributions by using circularly polarized light, as evident from Fig. 4.

C. Ar($3p_y$) initial state: Perpendicular alignment of the major polarization axis and the probed orbital

Now we address the case where the major polarization axis of the external field and the natural quantization axis of the probed orbital are orthogonal, the scenario illustrated in Fig. 3(b). To facilitate comparison with the results for the H($1s$) state, the major polarization axis of the external field is kept fixed along $\hat{x}$ and the Ar($3p_x$) state is rotated by 90° into the Ar($3p_y$) state. In this case, the peak electric field runs through the angular node of the probed orbital, and lowering the light ellipticity would result in increasing the electric field strength in the direction of the nodal plane. The resulting one-dimensional radial and angular plots are compared to those pertaining to the H($1s$) state in Fig. 5. The radial momentum distributions now show some, although rather small, differences between the H($1s$) and the Ar($3p_y$) states at ϵ different from $\pi/2$, i.e., for non-circularly polarized light. In the angular distributions, however, the differences are generally larger and in particular at $\epsilon = \pi/2$ (circular polarization limit). The vanishing density in the p_y orbital suppresses ionization at the peak of the pulse, thereby resulting in a bimodal angular distribution of electron momenta, in contrast to that for the H($1s$) state. By reducing light ellipticity, we see that the angular distributions retain bimodality down to $\epsilon = \pi/3$. The $\epsilon = \pi/4$ is disregarded in this discussion due to electron rescattering effects. The reason why the bimodal structure becomes less clear for decreasing ellipticity is that the increase in the field strength around the x direction starts compensating for the drop in density. As is known from tunneling theory [31,32] and the strong-field approximation [34,36–38], the rate of ionization is exponentially sensitive to the field strength while the shape of the orbital is reflected in the pre-exponential factor, and hence the over-all shape of the distribution is determined by a combination of these two factors. These findings indicate that with a proper alignment of the target system relative to the major polarization axis of the external field, information about the orbital symmetry can be obtained from the momentum distributions at a wider range of light ellipticity, but with clear preference for the case of circular polarization.

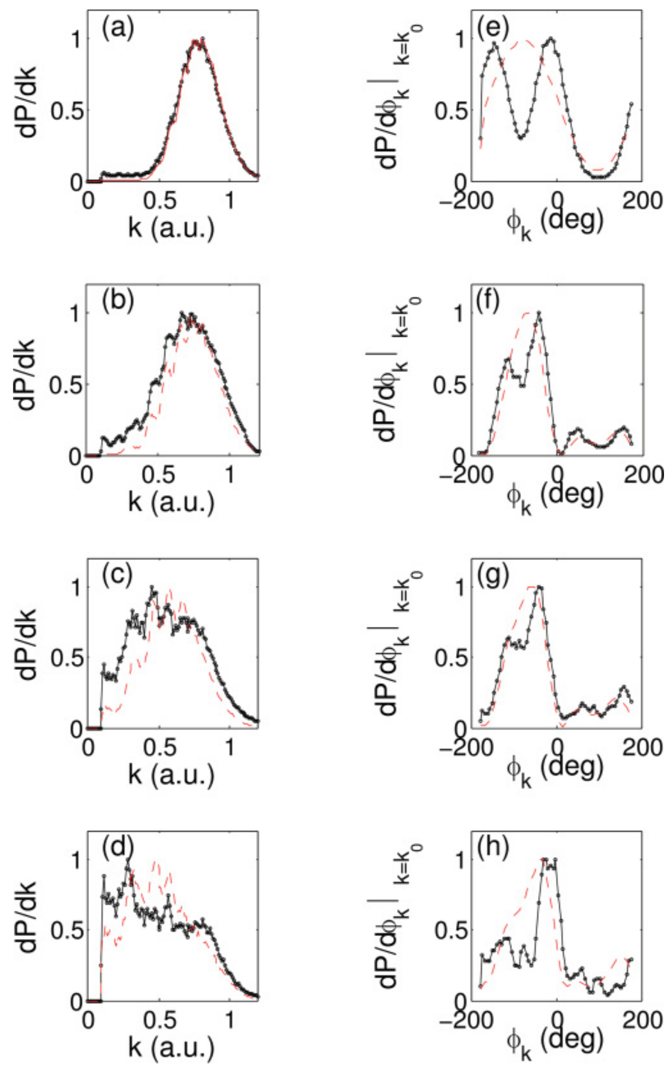

FIG. 5. (Color online) Radial momentum distributions (dP/dk, left column) and angular momentum distributions ($dP/d\phi_k\,|_{k=k_0}$, right column) for the H($1s$) state (red, dashed curves) and the Ar($3p_y$) state [black curves with circles, see Fig. 3(b)] at ϵ values of $\pi/2$ (top row), $11\pi/25$ (second row), $\pi/3$ (third row), and $\pi/4$ (bottom row). See caption of Fig. 2 for the values of the laser pulse parameters.

D. Effect of pulse duration

Now we investigate to what extent the above findings are sensitive to the duration of the laser pulse. In Fig. 6 we present radial and angular distributions of electron momenta for the Ar($3p_x$)/Ar($3p_y$) and the H($1s$) states obtained using seven-cycle instead of three-cycle pulses, keeping the light ellipticity in the range $\epsilon \in [\pi/2;\pi/4]$. For the Ar($3p_x$) [Ar($3p_y$)] state,

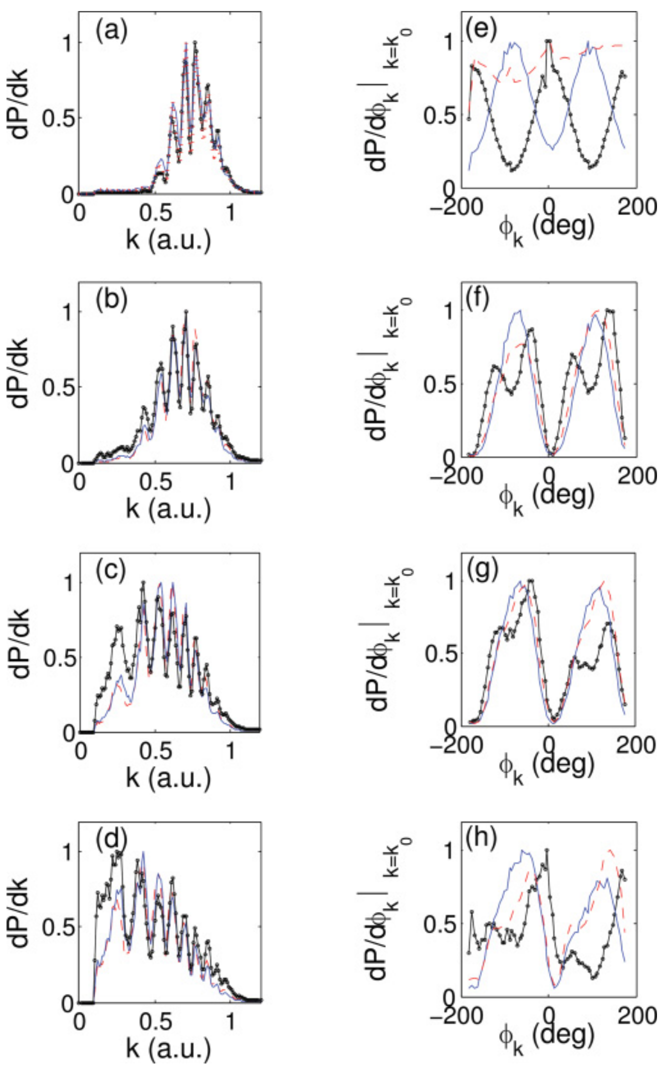

FIG. 6. (Color online) Radial momentum distributions (dP/dk, left column) and angular momentum distributions ($dP/d\phi_k\,|_{k=k_0}$, right column) for the H(1s) state (red, dashed curves), the Ar(3p_x) state [blue, solid curves, see Fig. 3(a)], and the Ar(3p_y) state [black curves with circles, see Fig. 3(b)] at ϵ values of $\pi/2$ (top row); $11\pi/25$ (second row); $\pi/3$ (third row) and $\pi/4$ (bottom row). The laser pulses contain seven cycles, $\omega = 0.057$ a.u. (800 nm), the CEP value is $\phi = -\pi/2$, and the peak intensity is 1.06×10^{14} W/cm^2.

we consider the parallel, cf. Fig. 3(a) [perpendicular, cf. Fig. 3(b)], alignment of the major polarization axis of the external field relative to the probed orbital.

For the Ar(3p_x) state, the radial momentum distributions [Figs. 6(a)–6(d)] are very similar to those for the H(1s) state. On the other hand, the angular distributions at $\epsilon = \pi/2$ [Fig. 6(e)] reproduce the angular density profiles except for a minor CEP effect and a $\pi/2$ phase factor: The electron density of the Ar(3p_x) [see Fig. 3(a)] peaks at $\phi_r = 0^\circ$ and 180° whereas the momentum distribution peaks at $\phi_k \approx -90^\circ$ and 90°, respectively. By going to smaller ellipticity values, the ionization probability will be reduced as the field points along the minor polarization axis ($\hat{y}$) and, hence, the angular distributions for the H(1s) and Ar(3p_x, 3p_y) states show a bimodal distribution in ϕ_k with a dip at $\phi_k = 0$ (corresponding to the $k_y = 0$ line), cf. Figs. 6(f)–6(h). From the figure, one can clearly see that the distributions pertaining to the H(1s) and Ar(3p_x) states are indistinguishable in the ellipticity range with minimal electron rescattering, that is, $\pi/2 > \epsilon \geqslant \pi/3$. Hence, in the case where the major polarization axis of the external field is aligned parallel to the probed orbital, the application of an elliptically polarized laser for interrogation of orbital symmetry is limited to the circular polarization case.

Turning to the case where the major polarization axis of the external field and the probed orbital are aligned perpendicular [Fig. 3(b)], the radial momentum distributions in Fig. 6 show small differences between the Ar(3p_y) and H(1s) states at ϵ in the range $[\pi/2;\pi/3]$, cf. Figs. 6(a)–6(c). What is more interesting is that the angular momentum distributions in Fig. 6 show distinct features of the Ar(3p_y) state, compared to the H(1s) state, at ϵ in the range $[\pi/2;\pi/3]$ where electron rescattering in minimal. These results are in agreement with those obtained in the few-cycle ionization regime, thereby showing that the main findings of this work are independent of the pulse duration.

IV. SUMMARY

In summary, we provide theoretical investigations of strong-field ionization from aligned atomic orbitals by elliptically polarized laser pulses. We focus on extracting information about the orbital symmetry (angular nodes) from the photoelectron momentum distributions, and how this information depends on light ellipticity, the angle between the major polarization axis of the external field and the probed orbital, and pulse duration (few-cycle vs many-cycle pulses). For orbitals with one angular node (p-type orbitals), the possibility of extracting information about the orbital angular structure from photoelectron momentum distributions computed at light ellipticity in the range $\epsilon \in [\pi/2;\pi/4]$ depends on the angle between the major polarization axis of the external field and the probed orbital. If the major axis of the external field is set parallel to the probed orbital, the imprints of the angular node can only be seen in the momentum distributions in the circular polarization case. On the contrary, by setting the major polarization axis of the external field perpendicular to the probed orbital, we find the imprint of the angular node in the momentum distribution over a wider range of light ellipticities. The results are independent of the pulse duration. We also note that for both H(1s) and Ar(3p), we found clear evidence in the momentum distributions for rescattering already at $\epsilon = \pi/4$.

The interest in using strong femtosecond pulses for investigations aiming at extracting information about orbital symmetry is not restricted to the case of isolated atoms or molecules starting out in their ground state. In fact it is much more interesting to think about larger molecules where much less is known. In such systems some nuclear dynamics is relatively slow and takes place on the picosecond time scale (see, e.g., Refs. [39,40] on control of torsional motion). In such cases the femtosecond pulses considered here may allow a very fast and time-resolved readout of the electronic orbital structure associated with a given nuclear configuration.

We note that time-resolved information about orbital symmetry could also in principle be extracted by using a short attosecond pulse leading to single-photon ionization.

At present, however, the attosecond pulses have a low intensity, making such probing experimentally challenging, and moreover attosecond pulse technology is still not as widespread as intense near-infrared femtosecond lasers. An alternative approach to the extraction of orbital information would be still to use 800-nm light but at a lower intensity. In that case the dynamics would be transferred away from the tunneling regime and into the multiphoton regime. In this regime the final momentum distributions would generally be more difficult to interpret due to the possible increase in the importance of intermediate states and symmetries thereof.

ACKNOWLEDGMENT

This work was supported by the Danish National Research Council (Grant No. 10-85430).

[1] J. L. Hansen, H. Stapelfeldt, D. Dimitrovski, M. Abu-samha, C. P. J. Martiny, and L. B. Madsen, Phys. Rev. Lett. **106**, 073001 (2011).
[2] P. Eckle, A. N. Pfeiffer, C. Cirelli, A. Staudte, R. Dorner, H. G. Muller, M. Buttiker, and U. Keller, Science **322**, 1525 (2008).
[3] P. Eckle, M. Smolarski, P. Schlup, J. Biegert, A. Staudte, M. Schoffler, H. G. Muller, R. Dorner, and U. Keller, Nat. Phys. **4**, 565 (2008).
[4] L. Holmegaard *et al.*, Nat. Phys. **6**, 428 (2010).
[5] H. Akagi, T. Otobe, A. Staudte, A. Shiner, F. Turner, R. Dorner, D. M. Villeneuve, and P. B. Corkum, Science **325**, 1364 (2009).
[6] W. Becker, F. Grasbon, R. Kopold, D. B. Milošević, G. G. Paulus, and H. Walther, Adv. At. Mol. Opt. Phys. **48**, 98 (2002).
[7] D. B. Milošević, G. G. Paulus, D. Bauer, and W. Becker, J. Phys. B **39**, R203 (2006).
[8] A. Staudte *et al.*, Phys. Rev. Lett. **102**, 033004 (2009).
[9] C. P. J. Martiny, M. Abu-samha, and L. B. Madsen, J. Phys. B **42**, 161001 (2009).
[10] M. Bashkansky, P. H. Bucksbaum, and D. W. Schumacher, Phys. Rev. Lett. **60**, 2458 (1988).
[11] S. Basile, F. Trombetta, and G. Ferrante, Phys. Rev. Lett. **61**, 2435 (1988).
[12] H. G. Muller, G. Petite, and P. Agostini, Phys. Rev. Lett. **61**, 2507 (1988).
[13] P. Lambropoulos and X. Tang, Phys. Rev. Lett. **61**, 2506 (1988).
[14] S. V. Popruzhenko, G. G. Paulus, and D. Bauer, Phys. Rev. A **77**, 053409 (2008).
[15] D. Dimitrovski *et al.* Phys. Rev. A **83**, 023405 (2011).
[16] J. L. Hansen *et al.*, Phys. Rev. A **83**, 023406 (2011).
[17] F. Filsinger, J. Küpper, G. Meijer, L. Holmegaard, J. H. Nielsen, I. Nevo, J. L. Hansen, and H. Stapelfeldt, J. Chem. Phys. **131**, 064309 (2009).
[18] L. Holmegaard, J. H. Nielsen, I. Nevo, H. Stapelfeldt, F. Filsinger, J. Küpper, and G. Meijer, Phys. Rev. Lett. **102**, 023001 (2009).
[19] I. Nevo, L. Holmegaard, J. H. Nielsen, J. L. Hansen, H. Stapelfeldt, F. Filsinger, G. Meijer, and J. Küpper, Phys. Chem. Chem. Phys. **11**, 9912 (2009).
[20] S. S. Viftrup, V. Kumarappan, L. Holmegaard, C. Z. Bisgaard, H. Stapelfeldt, M. Artamonov, E. Hamilton, and T. Seideman, Phys. Rev. A **79**, 023404 (2009).
[21] P. B. Corkum, Phys. Rev. Lett. **71**, 1994 (1993).
[22] C. P. J. Martiny, M. Abu-samha, and L. B. Madsen, Phys. Rev. A **81**, 063418 (2010).
[23] T. K. Kjeldsen and L. B. Madsen, J. Phys. B **37**, 2033 (2004).
[24] J. Muth-Böhm, A. Becker, and F. H. M. Faisal, Phys. Rev. Lett. **85**, 2280 (2000).
[25] E. B. Tulenko and B. A. Zon, Las. Phys. **13**, 450 (2003).
[26] H. G. Muller and F. C. Kooiman, Phys. Rev. Lett. **81**, 1207 (1998).
[27] T. K. Kjeldsen, L. A. A. Nikolopoulos, and L. B. Madsen, Phys. Rev. A **75**, 063427 (2007).
[28] L. B. Madsen, L. A. A. Nikolopoulos, T. K. Kjeldsen, and J. Fernandez, Phys. Rev. A **76**, 063407 (2007).
[29] P. Dietrich, F. Krausz, and P. B. Corkum, Opt. Lett. **25**, 16 (2000).
[30] C. P. J. Martiny and L. B. Madsen, Phys. Rev. Lett. **97**, 093001 (2006).
[31] N. B. Delone and V. P. Krainov, J. Opt. Soc. Am. B **8**, 1207 (1991).
[32] V. S. Popov, Phys. Usp. **47**, 855 (2004).
[33] C. P. J. Martiny and L. B. Madsen, Phys. Rev. A **76**, 043416 (2007).
[34] L. V. Keldysh, Zh. Eksp. Teor. Fiz. **47**, 1945 (1964) [Sov. Phys. JETP **20**, 1307 (1965)].
[35] M. Abu-samha, D. Dimitrovski, and L. B. Madsen, J. Phys. B **41**, 245601 (2008).
[36] F. H. M. Faisal, J. Phys. B **6**, L89 (1973).
[37] H. R. Reiss, Phys. Rev A **22**, 1786 (1980).
[38] D. Dimitrovski, C. P. J. Martiny, and L. B. Madsen, Phys. Rev. A **82**, 053404 (2010).
[39] C. B. Madsen, L. B. Madsen, S. S. Viftrup, M. P. Johansson, T. B. Poulsen, L. Holmegaard, V. Kumarappan, K. A. Jørgensen, and H. Stapelfeldt, Phys. Rev. Lett. **102**, 073007 (2009).
[40] C. B. Madsen, L. B. Madsen, S. S. Viftrup, M. P. Johansson, T. B. Poulsen, L. Holmegaard, V. Kumarappan, K. A. Jørgensen, and H. Stapelfeldt, J. Chem. Phys. **130**, 234310 (2009).